FBXW7 regulates endothelial barrier function by suppression of the cholesterol synthesis pathway and prenylation of RhoB

Manon C.A. Pronk[1], Jisca Majolée[1], Anke Loregger[2], Jan S.M. van Bezu[1], Noam Zelcer[2], Peter L. Hordijk[1], Igor Kovačević[1]*

[1] Department of Physiology, Amsterdam Cardiovascular Sciences, Amsterdam University Medical Centers, location VUmc, Amsterdam, The Netherlands

[2] Department of Medical Biochemistry, Amsterdam University Medical Centers, location AMC, Amsterdam, The Netherlands

* Corresponding author

E-mail: i.kovacevic@vumc.nl

Abstract

Rho GTPases control both the actin cytoskeleton and adherens junction stability and are recognized as essential regulators of endothelial barrier function. Rho GTPases act as molecular switches and are primarily regulated by the exchange of GDP and GTP. However, post-translational modifications such as phosphorylation, prenylation and ubiquitination can additionally alter their localization, stability and activity. F-box proteins are involved in the recognition of substrate proteins pre-destined for ubiquitination and subsequent degradation. Given the importance of ubiquitination we studied the effect of loss of 62 members of the F-box protein family on endothelial barrier function in human umbilical vein endothelial cells (HUVECs). Endothelial barrier function was quantified by Electrical Cell impedance sensing (ECIS) and

macromolecule passage assay. Our RNAi-based screen identified FBXW7 as a key regulator of endothelial barrier function. Mechanistically, loss of FBXW7 induced the accumulation of the RhoB GTPase in endothelial cells, resulting in their increased contractility and permeability. FBXW7 knockdown induced activation of the cholesterol biosynthesis pathway and changed the prenylation of RhoB. This effect was reversed by farnesyl transferase inhibitors and by the addition of geranylgeranyl pyrophosphate.

In conclusion, this study identifies FBXW7 as a novel regulator of endothelial barrier function *in vitro*. Loss of FBXW7 indirectly modulates RhoB activity via alteration of the cholesterol biosynthesis pathway and, consequently, of the prenylation status and activity of RhoB, resulting in increased contractility and disruption of the endothelial barrier.

Introduction

Endothelial cells (ECs) line all blood and lymph vessels throughout the body. They form a monolayer of tightly adherent cells which regulates the transmigration of leukocytes and transport of plasma proteins from the circulation into the tissues. Proper function of the endothelial barrier is crucial, as its dysfunction is a hallmark of chronic inflammatory diseases which can result in edema and tissue damage (1). Adherens junctions (AJs) serve as a bridge connecting the actin cytoskeleton of neighboring endothelial cells (2) and are composed of multiple proteins including the transmembrane protein Vascular Endothelial-cadherin (VE-cadherin) and intracellular adaptor proteins such as α- and β-catenin, which link VE-cadherin to the actin

cytoskeleton (3). Importantly, the dynamics of the cytoskeleton, allowing force-generation parallel or perpendicular to cell-cell contacts, can stabilize or disrupt AJs (4, 5).

Important regulators of AJs and of the actin cytoskeleton are the Rho GTPases. It is well-established that Rac1 and Cdc42 promote endothelial barrier stability (6), while RhoA activation leads to endothelial barrier disruption (7). Activity of Rho GTPases is primarily regulated by a conformational change that is dependent on GDP or GTP binding (8). The GTP-bound conformation enables interaction with downstream signaling proteins. Rho GTPases are activated by Guanine-nucleotide Exchange Factors (GEFs) which promote the exchange of GDP for GTP and by GTPase Activating Proteins (GAPs) which stimulate the hydrolysis of GTP, leading to GTPase inactivation (9). Inactive Rho GTPases are protected from ubiquitin-dependent degradation by binding to guanine-nucleotide dissociation inhibitor (GDIs) in the cytosol (10). It has become increasingly clear that nucleotide binding and the interaction with GEFs and GAPs is one of several mechanisms which regulate Rho GTPase activity as Rho GTPases can also be phosphorylated, prenylated and ubiquitinated to fine-tune their function (11, 12).

Among these post-translational modifications, prenylation of Rho GTPases is a key determinant of their function. Prenylation targets Rho GTPases to the correct subcellular location, and is important for interactions with regulatory proteins and downstream signaling effectors. RhoB is unique among the Rho GTPases because it can be both geranylgeranylated and farnesylated (13). Farnesyl and geranylgeranyl are isoprenoids that are generated through the cholesterol synthesis pathway and that are covalently attached to the CAAX-box at the C-terminus of Rho GTPases through the activity of the enzymes farnesyl transferase (FTase) and geranylgeranyl

transferase I (GGTase-I), respectively. Tshe geranylgeranylated form of Rho GTPases is targeted for proteolysis (14), and is considered to be inactive while the farnesylated form is active (15). Accordingly, inhibition of farnesylation of RhoB was shown to reduce vascular cell proliferation, increase endothelium-dependent vasodilatation and reduced vasoconstriction of pulmonary arteries in an animal model of hypoxia-induced pulmonary hypertension (16).

Besides prenylation, ubiquitination is an important post-translational modification which regulates the protein stability of both RhoA and RhoB (17, 18). During the ubiquitination process, the small protein ubiquitin (76 amino acids) is covalently attached to substrate proteins to selectively target them to the proteasome or to lysosomes for degradation. Ubiquitination consists of 3 steps whereby ubiquitin is activated by an E1 ubiquitin enzyme, transferred to an ubiquitin-conjugating enzyme E2, and attached to a substrate as mono-ubiquitin or a poly-ubiquitin by an E3 ligase (19). The E3 ligases are characterized by several defining motifs which allow direct or indirect ubiquitination of substrates (20). One family of E3 ligases, the Cullin RING (Really Interesting New Gene) ligases form large protein complexes; the SKP1-Cullin1-FBP (SCF)-ligase is a well-characterized example (21). In this complex, Cullin-1 is the central adaptor protein which interacts via Rbx1 with the E2 ubiquitin ligase and with the F-box protein via Skp1. In this E3 ligase complex the F-box protein acts as a specific recognition receptor that dictates the substrates for ubiquitination and subsequent degradation. The F-box family contains three groups of proteins, which are named according to their structure; the FBWs contain a WD-40 repeat, the FBLs contain a Leucine-rich repeat and the FBXs which do not contain a WD-40 or Leucine-rich repeat but often have other protein-protein interaction domains. A central question pertaining to F-box proteins is resolving the function of

each individual F-box protein family member. The members which have been studied so far are mostly associated with the control of proliferation via the degradation of cyclins (21). Due to their structural diversity, F-box proteins can bind several different substrate proteins and are involved in the pathogenesis of various human diseases including Parkinson's disease and cancer (22, 23). Besides the function of FBXW7 in angiogenesis and inflammation (24, 25), the role of other F-box proteins in endothelium was not studied in detail.

In the current study, we aimed to determine if F-box proteins play a role in endothelial barrier function. Using primary HUVECs in combination with esiRNA-mediated knockdown of F-box proteins, we found that FBXW7 is involved in regulation of the endothelial barrier. We further showed that cells lacking FBXW7 had a contractile phenotype which results in reduced barrier function and increased permeability both in resting and thrombin-stimulated cells. This phenotype can be attributed to the increased abundance of the contraction-inducing RhoB GTPase. Concomitantly, we found that FBXW7 depletion induced activation of the cholesterol synthesis pathway in endothelial cells and thereby impaired both the prenylation and degradation of RhoB.

Results

esiRNA screen of Fbox proteins identified both positive and negative regulators of endothelial barrier function

To identify new ubiquitination regulators which are important for endothelial barrier function, we screened a custom library of esiRNAs (Sigma) targeting 62 F-box proteins in primary HUVECs (Human Umbilical Vein endothelial cells). The targets comprise members of all three different classes of F-box proteins (Table 1). Electrical Cell-substrate Impedance Sensing (ECIS) was used to measure endothelial barrier function of HUVECs before, during and after transfection with esiRNAs. The screen was repeated 4 times with 4 different pools of HUVECs, each derived from 3 different donors. The endothelial barrier function was measured in real time for 72 hours after transfection and was then evaluated (Figure 1A). For data analysis, the mean delta increase in endothelial barrier resistance of each F-box protein esiRNA was compared to the mean delta increase of the control. The only significant hit in this screen after false discovery rate (FDR) correction was F-box/WD repeat-containing protein 7 (FBXW7) depicted in red ($p=0.0079$) (Figure 1B). Other proteins which showed a significant effect before FDR correction were FBXL19, FBXL17, FBXL16, FBXO18 and FBXO28. However, some of the tested F-box proteins showed large intra-experimental variation, which could have influenced the interpretation of the results. Most of the tested F-box protein siRNAs did not show large effects compared to the si-EGFP control. This might be due to redundancy between F-box proteins or their irrelevance for regulation of endothelial barrier function. While loss of FBXW7 showed the largest decrease in barrier function, depletion of FBXL19 induced the largest increase in barrier function (Figure 1C). The effects of FBXW7 and FBXL19 esiRNAs were corroborated by lentivirally expressed shRNAs targeting the same

proteins (Supplemental Figure 1). These findings indicate that a limited subset of F-box proteins is involved in the regulation of the endothelial barrier, and that FBXW7 is a positive regulator of endothelial barrier function.

FBXW7 knockdown impairs endothelial barrier function

To expand the results from the esiRNA screen, we repeated the experiments with independent siRNAs (ON-TARGET plus SMART pools) in different pools of primary HUVECs. As control in these experiments, cells were transfected with non-targeting siRNA (siNT). First, we confirmed that FBXW7 mRNA was effectively downregulated in cells which were transfected with FBXW7 siRNA. Figure 2A shows that there is approximately 95% loss of FBXW7 mRNA in FBXW7 knockdown cells. SiRNA-mediated loss of FBXW7 in endothelial cells resulted in a significantly decreased barrier resistance compared to control cells (Figure 2B,C). Resolving the endothelial resistance measurements into separate components reflecting cell-cell and cell-matrix interaction(26) showed that loss of FBXW7 did not significantly change cell-matrix interaction compared to control cells (Figure 2D,E). However, the cell-cell interaction was significantly lower in FBXW7 knockdown cells compared to control cells (Figure 2F,G). Because the endothelial resistance measurements showed significant effects on cell-cell interaction we next focused on the morphology of the actin cytoskeleton and adherens junctions in FBXW7 knockdown cells. Phalloidin staining showed more intense overall F-actin staining and formation of contractile actin rings in FBXW7 knockdown cells (Figure 2H). Furthermore, immunostaining of the cell-cell adhesion protein VE-cadherin revealed discontinuous VE-cadherin distribution in FBXW7-depleted cells (Figure 2H). These findings were confirmed by use of an shRNA targeting FBXW7 (Supplemental Figure 2). Furthermore, we analyzed the co-localization of VE-cadherin and F-actin. This analysis showed that

co-localization of VE-cadherin and F-actin is significantly lower in FBXW7 knockdown cells compared to control cells (Figure 2I,J). Finally, FBXW7 knockdown did not significantly reduce the number of endothelial cells at 72 hours post-transfection (Figure 2K). Together, these findings suggest that decreased barrier function in FBXW7 knockdown cells is induced by increased stress fiber formation and loss of stable, junctional VE-cadherin distribution.

Loss of FBXW7 delays recovery from thrombin-induced loss of barrier integrity.

In the human circulation, the endothelium can become exposed to numerous vaso-active agents. Here we studied the effect of the pro-inflammatory protease thrombin on endothelial barrier function in control and FBXW7 knockdown cells. The ability of the cells to recover their barrier function after thrombin stimulation is another parameter which gives information about endothelial junction dynamics. Stimulation with thrombin (1 U/mL) resulted in a rapid drop in endothelial barrier resistance (Figure 3A). This drop in resistance was not significantly different between control and FBXW7 knockdown cells (Figure 3B). In contrast, the recovery after thrombin stimulation at 3 hours post stimulation was significantly reduced in FBXW7 knockdown cells (Figure 3C).

To test the effect of thrombin on the endothelial barrier in an independent assay, we measured macromolecule passage across endothelial monolayers, stimulated with thrombin. In line with the ECIS results, the FBXW7 knockdown cells displayed increased HRP leakage compared to control cells under basal conditions (Figure 3D). Stimulation with thrombin increased overall permeability of the monolayer, which was enhanced in cells lacking FBXW7. The permeability of FBXW7 knockdown cells was

higher compared to the control cells at all time points with statistically significant difference at 1.5 and 2 hours after thrombin stimulation (Figure 3D).

In order to analyze if the effect on permeability correlated with changes in cell morphology, we visualized F-actin and VE-cadherin in control and FBXW7 siRNA transfected cells. 15 Minutes after thrombin addition we observed gaps and stress fiber formation in monolayers of both control and FBXW7 knockdown cells. However, the gaps appeared larger and the intensity of the F-actin contractile ring was higher in FBXW7 knockdown cells compared to control cells (Figure 3E, I). Both FBXW7 knockdown and control cells displayed discontinuous and jagged VE-cadherin staining (Figure 3E), without significant difference in overall VE-cadherin levels (Figure 3G). 3 hours after thrombin treatment we observed that control cells, although they still contained stress fibers, did not show inter-endothelial gaps anymore and that VE-cadherin distribution was more continuous and concentrated (Figure 3F). In contrast, gaps were still present in the monolayer of FBXW7 knockdown cells (Figure 3J). Additionally, at 3 hours after thrombin treatment FBXW7 knockdown cells showed less intense and discontinuous VE-cadherin staining compared to the control cells (Figure 3F, H). In conclusion, FBXW7 knockdown cells recover at a slower rate after thrombin stimulation, possibly due to increased stress fiber formation and VE-cadherin turnover.

FBXW7 depletion increases RhoB levels

The increased formation of F-actin stress fibers which we observed in FBXW7 knockdown cells could be caused by increased expression and/or activity of Rho GTPases. Previously, RhoA was shown to be an important regulator of contraction induced by thrombin stimulation(7). We recently showed that besides RhoA, RhoB

mediates the contraction of endothelial cells(27) and we therefore analyzed RhoB protein abundance. We found that FBXW7 knockdown cells showed a markedly increased level of RhoB compared to control cells (Figure 4A). In contrast, RhoA and to lesser extent RhoC levels were reduced upon FBXW7 depletion (Figure 4A). To exclude the possibility that the effects we observe on RhoB levels in FBXW7 knockdown cells are unspecific, we performed a rescue experiment. In this experiment we depleted FBXW7 by using lentiviruses encoding an shRNA which targets the 3'UTR of the FBXW7 mRNA. In accordance with siRNA experiments we found that shFBXW7 also increases RhoB expression in these experiments (Figure 4B). Ectopic re-expression of FBXW7 from a doxocycline-inducible lentiviral vector reduced the expression of RhoB to the levels found in control cells. To test if the increase in RhoB in FBXW7 knockdown cells was the main cause of the decreased barrier function, we performed the knockdown of FBXW7 in combination with loss of RhoA or of RhoB. We found that loss of RhoB significantly increased endothelial barrier resistance, while RhoA knockdown did not show differences compared to control cells (Figure 4C,D). Depletion of FBXW7 decreased endothelial barrier significantly compared to control cells, which is in line with the data in Figure 2. Combined knockdown of FBXW7 and RhoA induced a similar decrease in endothelial barrier resistance as the single FBXW7 knockdown. On the other hand, endothelial resistance measured in cells with double knockdown of FBXW7 and RhoB was not significantly different compared to control cells (Figure 4C,D). In additional experiments we tested if single siRNA sequences targeting FBXW7 similarly enhanced RhoB expression and disrupted endothelial barrier function as we observed with siRNA pool. We found that 2 out of 4 tested clones indeed increased the levels of RhoB which was accompanied by a significant loss of endothelial barrier

integrity (Supplemental Figure 3 A,B). Since subcellular targeting of Rho GTPases is important for their function, we analyzed RhoB localization in control and FBXW7 knockdown cells by confocal microscopy. In line with immunoblotting, immunostaining for RhoB showed that FBXW7 knockdown cells contained more RhoB localized to vesicles compared to control cells (Figure 4E). In summary, our results indicate that the decrease of endothelial barrier integrity induced by the loss of FBXW7 expression is to a large extent the result of increased levels of RhoB protein.

Loss of FBXW7 activates the cholesterol synthesis pathway in endothelial cells

In previous studies, FBXW7 was shown to regulate ubiquitination and abundance of RhoA in gastric cancer (28). We recently found that another CRL complex, namely Cullin-3/KCTD10, is responsible for RhoB ubiquitination in endothelial cells (18). We tested if ubiquitination of RhoB is also regulated by FBXW7. Using an *in vivo* ubiquitination assay in HEK293T cells, we did not observe an increase in RhoB ubiquitination upon co-expression of FBXW7 (Supplemental Figure 4A). In accordance with this, we also did not observe reduced ubiquitination of endogenous RhoB in FBXW7 depleted endothelial cells (Supplemental Figure 4B).

FBXW7 has previously been demonstrated to control the cholesterol biosynthesis pathway in hepatocytes owing to its ability to regulate the level of the sterol-regulatory element binding protein (SREBP) transcription factors (29, 30). To test if this is also the case in endothelial cells, we measured mRNA levels of several proteins which are part of the cholesterol pathway. In line with FBXW7 having a similar effect in ECs, its loss leads to increased expression of the SREBP-regulated target genes 3-hydroxy-3-methyl-glutaryl-coenzyme A reductase (*HMGCR*). Squalene synthase (SQS), squalene epoxidase (SQLE) and the low-density

lipoprotein receptor (LDLr) (Figure 5A-D). For two of these genes we tested if increased mRNA expression also resulted in increased abundance of the encoded protein. We found that mirroring the effects on mRNA levels, the protein abundance of SQLE was increased 2.5-fold in FBXW7 knockdown cells compared to control cells. Similarly, LDLR levels were increased 2-fold in FBXW7 knockdown cells compared to control cells (Figure 5E). This data is in line with a previous publication, in which FBXW7 knockdown was shown to lead to the activation of SREBPs in U2OS and HCT116 epithelial cancer cells (30), and activation of the cholesterol synthesis pathway. Together, these findings indicate that FBXW7 knockdown leads to the upregulation of several components of the cholesterol synthesis pathway in endothelial cells.

Stimulation of geranylgeranylation rescues disruption of endothelial barrier in FBXW7 knockdown cells

RhoB in endothelial cells is mostly localized in vesicles, however, inhibition of RhoB ubiquitination re-distributes RhoB predominantly to the plasma membrane (18). In Figure 4B, we demonstrated that in FBXW7 knockdown cells, the level of RhoB was increased with the protein localizing both to and outside of the vesicles. This finding, in combination with the upregulation of the cholesterol pathway, led us to hypothesize that prenylation might play a role in re-distribution of RhoB upon FBXW7 knockdown. Previously, it was shown that the cholesterol synthesis pathway and prenylation of RhoB are crucial for the regulation of RhoB levels (31). RhoB can be either farnesylated by farnesyl transferase or geranylgeranylated by geranylgeranyl transferase. Therefore, we treated control and FBXW7 knockdown cells for 24 hours with a farnesyl transferase inhibitor (FTI), a geranylgeranyl transferase inhibitor (GGTI), or a combination of both at 48 hours after transfection. In control cells, we

observed no differences in endothelial resistance following treatment with FTI. Although the addition of GGTI alone or in combination with FTI induced an initial drop in electrical resistance, there were no statistically significant differences at 24 hours after addition (Figure 6A,B). As expected, FBXW7 knockdown cells without stimulation showed a drop in resistance in the 24 hours during which they were monitored (Figure 6C,D). When FTI was added to the FBXW7 knockdown cells, this drop was largely reversed, while addition of GGTI alone or GGTI in combination with FTI did not show any differences as compared to untreated FBXW7 knockdown cells (Figure 6C,D).

In subsequent experiments we analyzed the effects of FTI and GGTI on RhoB protein levels. In untreated FBXW7 knockdown cells we found increased levels of RhoB. Treatment with FTI slightly increased RhoB levels in control cells but did not further increase RhoB in FBXW7 knockdown cells. Addition of GGTI to control cells, as well as combined treatment with FTI and GGTI, induced a more robust increase in RhoB protein levels compared to FTI treatment (Figure 6E).

Since prenylation is important for the localization of RhoB (14), we analyzed RhoB by immunofluorescence after addition of the inhibitors. FBXW7 knockdown cells resulted in more RhoB protein, stress fiber formation and decreased VE-cadherin expression at the cell-cell contacts (Figure 6F; see also Figure 2). Treatment with FTI partially reduced stress fiber formation and restored the VE-cadherin distribution in FBXW7 knockdown cells (Figure 6F). Treatment with GGTI and the combined treatment of FTI and GGTI resulted in increased, homogeneously distributed RhoB throughout the cell in both control and FBXW7 knockdown cells. In the FBXW7 knockdown cells we observed decreased VE-cadherin intensity as compared to control cells (Figure 6F). Since addition of FTI protected against the barrier disruptive effect of the loss of

FBXW7, possibly by induction of geranylgeranylation of RhoB, we hypothesized that addition of geranylgeranyl pyrophosphate (GGPP) might also restore the disruptive effect of FBXW7 knockdown. Indeed, addition of GGPP resulted in the restoration of barrier function in FBXW7 knockdown cells to control cell levels, while addition of farnesyl pyrosphosphate (FPP) did not show any significant effects (Figure 6G). Together, these data suggest that due to the increased generation of isoprenoids originating from the cholesterol synthesis pathway, which is induced upon FBXW7 knockdown, RhoB is increasingly farnesylated which results in the accumulation of (active) RhoB in endothelial cells.

RhoB prenylation is impaired in FBXW7 knockdown cells

Changes in protein prenylation can be assessed by analyzing the lipophilic properties of the protein using Triton X-114 extraction. This method was recently applied to study prenylation of Rab7 in neurons (32). First, we tested if distribution of RhoB between detergent-rich lipophilic and aqueous hydrophilic fraction is changed upon application of GGTI or FTI. We found that in unstimulated cells, RhoB is predominantly detected in the detergent rich lipophilic fraction (Figure 7A). Treatment of endothelial cells with GGTI resulted in a complete shift of RhoB towards aqueous fraction. In contrast, FTI did not change the distribution of RhoB between the aqueous and detergent-rich fraction. Then we analyzed the distribution of RhoB in FBXW7 knockdown cells and we found that the fraction of RhoB in the aqueous fraction was increased 2 fold when compared to control cells (Figure 7B,C). Increased RhoB in this fraction in FBXW7 knockdown cells partially mimics geranylgeranyl transferase inhibition. In contrast to RhoB, RhoA and RhoC are detected predominantly in the aqueous fraction and their lipophilic properties were not affected by FBXW7 knockdown.

In summary, our data suggest a novel model of the regulation of endothelial barrier function by FBXW7 (Figure 8). Knockdown of FBXW7 leads to increased activation of the cholesterol synthesis pathway, likely a result of SREBP stabilization (30). In this setting, there is more GGPP and FPP available for prenylation, and as a consequence, RhoB is both more geranylgeranylated and farnesylated. Since farnesylated RhoB is protected from degradation (16), the amount of active RhoB increases, leading to increased stress fiber formation and barrier disruption. FTI can counteract this effect by switching the equilibrium towards geranylgeranylation of RhoB which drives inactive RhoB to vesicles. Addition of GGPP rescues the siFBXW7-phenotype since this promotes geranylgeranylation of RhoB (Figure 8).

Discussion

Here we report the result of an ECIS-based screen of esiRNA-mediated depletion of 62 F-box proteins in HUVEC. Our data show that in this protein family FBXW7 is a key positive regulator of endothelial barrier function. Knockdown of FBXW7 in resting endothelial cells induces stress fiber formation and contractile actin ring formation, causing decreased barrier function both in resting and thrombin-stimulated cells. Depletion of FBXW7 also leads to upregulation of RhoB protein levels and activation of the cholesterol synthesis pathway. The latter pathway is the source of isoprenoids which are crucial modifiers of RhoB localization, activity and stability (13, 14). These findings suggest that RhoB prenylation might be affected in FBXW7 knockdown cells which could result in increased activity of RhoB and subsequent disruption of the endothelial barrier.

In parallel, we found that RhoA and RhoC levels were decreased in FBXW7 knockdown cells. This might be caused by the regulatory interactions that exist between RhoA, RhoB and RhoC, affecting their respective expression levels (27). An si-RNA based F-box protein screen was previously performed to assess their effect on virus replication (33) and cell proliferation in several types of cancers (34, 35). However, our study is the first one to analyze the function of F-box proteins in the regulation of the endothelial barrier. *In vivo* work of Izumi et al. showed that an endothelial specific knockout of FBXW7 leads to increased activation of the Notch pathway which results in decreased angiogenesis (24). In addition, Tsunematsu et al. described that FBXW7 knockout mice are not viable due to impaired vascular development (36). FBXW7 was also shown to be involved in regulation of angiogenesis, via ubiquitination of KLF2 in endothelial cells (25). Together, these previous findings already indicate that FBXW7 is an important pleiotropic regulator of vascular dynamics.

We recently reported that knockdown of FBXW7 by short hairpin RNAs leads to increased stress fiber formation (18). Also, we found that inhibition of ubiquitination greatly increased the level of RhoB in endothelial cells. In this situation, RhoB localizes diffusely throughout the cells and at the plasma membrane (18). In the current study, we show that RhoB protein is increased and mainly detected in vesicles upon loss of FBXW7. This suggests that besides ubiquitination of RhoB, additional mechanisms might regulate RhoB localization upon depletion of FBXW7 in endothelial cells.

Given the known function of FBXW7 in controlling SREBP ubiquitination (29, 30), we tested if the cholesterol synthesis pathway is affected in FBXW7 knockdown HUVEC (29). Indeed, we found an increase in the SREBP-2-regulated program in siFBXW7

transfected endothelial cells. This is in good agreement with data from Sundqvist et al. who showed that depletion of FBXW7 stabilized SREBP in the nuclei of HCT116 cells and increased expression of SREBP target genes like *LDLR* and *HMGCR* (30). The same effect was described by Onoyama et al. who found that knockdown of FBXW7 leads to liver steatosis and hamartoma development, due to hepatic accumulation of lipids (37).

FBXW7 regulates degradation of numerous target proteins (*e.g.* SREBP-1 and -2, Myc, Notch-1, and cyclin E) and this promiscuity of FBXW7 hinders clear dissection of the molecular mechanism behind the endothelial barrier disruption in FBXW7 depleted cells. Nevertheless, by using low proliferating, close to confluent primary human endothelial cells in low passages, we minimalized potential effects of FBXW7 loss on cell proliferation. Clear upregulation of the cholesterol synthesis pathway, rescue of the phenotype by enhanced geranylation and RhoB depletion all suggest that the impairment in the FBXW7-prenylated RhoB signaling axis plays a major role in disruption of endothelial barrier integrity upon FBXW7 depletion.

Farnesyl transferase inhibitors (FTIs) and geranylgeranyl transferase inhibitors (GGTIs) were previously used to study the effects of prenylation on expression and localization of RhoB. These studies have shown that FTI induces a shift towards geranylgeranylated RhoB, while GGTI leads to a shift towards farnesylated RhoB. As described previously, geranylgeranylated RhoB is localized in vesicles (14, 38). Immunofluorescent stainings in this study revealed that RhoB is localized in vesicles in FBXW7 knockdown cells which resembles localization of RhoB in control cells treated with FTI. This suggests that there is more geranylgeranylated RhoB in FBXW7 knockdown cells when compared to control cells. Interestingly, addition of FTI to FBXW7 cells slightly decreased the levels of RhoB suggesting that there is

also farnesylated RhoB in FBXW7 knockdown cells and that farnesylation might protect RhoB from degradation. In accordance with this, addition of GGTI to the control and FBXW7 knockdown cells caused an increase in RhoB protein levels and localization of RhoB outside vesicles. GGTI treatment also caused a re-distribution of RhoB from detergent-rich lipophilic cell lysate fraction to aqueous hydrophilic fraction. This was to some degree similar in FBXW7 knockdown cells, where RhoB was also increased in the aqueous hydrophilic fraction. These findings suggesting that both farnesylation and geranylgeranylation of RhoB are impaired in FBXW7 knockdown cells.

Knockdown of FBXW7 and/or stimulation with FTI and GGTI resulted in differential effects on actin stress fiber formation. The increased stress fiber formation in FBXW7 knockdown cells is likely due to increased expression of RhoB, as RhoB promotes stress fiber formation (27). There is evidence that geranylgeranylated RhoB (39) as well as farnesylated RhoB can induce stress fiber formation (16). Since FTI treatment or supplementation of cell medium with GGPP partially rescue the contractile phenotype and loss of endothelial integrity in FBXW7 knockdown cells it is conceivable that the major form of RhoB which induces contraction is not the geranylgeranylated, but the farnesylated one. FTI application promotes the switch towards the geranylgeranylated form of RhoB which is translocated to intracellular vesicles for degradation. In contrast, addition of GGTI increases the farnesylated form of RhoB which is less efficiently degraded and may induce contraction.

In conclusion, we found that perturbations in the FBXW7-regulated cholesterol synthesis pathway and consequently protein prenylation disrupt endothelial integrity. Altered prenylation of RhoB upon FBXW7 knockdown appears to be the main cause

of this effect. This indicates that tight regulation of the expression and activity of RhoB levels is essential for the maintenance of endothelial integrity.

Disclosure of Potential Conflicts of Interest

No potential conflicts of interest were disclosed.

Funding Details

IK was supported by a grant (#1311) of the Landsteiner Foundation for Blood Transfusion Research (LSBR). MCAP was funded by the Rembrandt Institute for Cardiovascular Science. NZ is an Established Investigator of the Dutch Heart Foundation (2013T111) and is supported by an ERC Consolidator grant (617376) from the European Research Council and by a Vici grant from the Netherlands Organization for Scientific Research (NWO; 016.176.643). AL is supported by a Dekker grant from the Dutch Heart Foundation (2016T015). This work was supported by an Amsterdam Cardiovascular Sciences (ACS) “out of the box grant” to NZ and PLH.

Author contributions

IK, PLH and NZ conceived the project and designed experiments. MCAP, JM, AL and IK designed and performed experiments and analyzed data. JSMvB performed experiments. MCAP, JM, IK, AL, NZ and PLH wrote the manuscript.

Material & Methods

Antibodies, reagents and si-RNAs

The following antibodies were used for immunostaining: αVE-cadherin XP (#2500) (Cell Signaling Technologies, Danvers, MA), and (#sc-8048) (Santa Cruz biotechnology, Santa Cruz, CA); Dapi (Thermo Fisher scientific). Alexa 488-secondary antibody (anti-rabbit and anti-mouse) and Alexa 647 – secondary antibody (anti-rabbit) (All invitrogen) were the secondary antibodies.

The following antibodies were used for protein analysis: ß-actin (Merck), low-density lipoprotein receptor (LDLR; Biovision), squalene epoxidase (SQLE; Proteintech). αp44/42 MAPK (ERK1/2)(#9102), αRhoA (#2117), αRhoC (#3430) and αGAPDH (#2118)(Cell Signaling Technologies), αRhoB (#sc-180 and sc-8048)(Santa Cruz biotechnology, Santa Cruz, CA), αHA (H3663) and αVinculin (V4139) (Sigma Aldrich), αFbxw7 (ab171961)(Abcam) and mouse αUbiquitin (FK-2) (Boston Biochem). As secondary antibody horseradish peroxidase-conjugated goat-anti rabbit antibody and goat-anti mouse (Dako) were used.

For inhibition of geranylgeranylation and farnesylation, GGTI-298 and FTI-277 HCL (Both Selleck chemicals) were used. In order to normalize prenylation the in FBXW7 knockdown cells geranylgeranyl pyrophosphate (GGPP) or farnesyl pyrophosphate (FPP) were applied (Sigma).

The small interference RNAs (siRNAs) which were used are: ON-TARGET plus Non-targeting pool (siNT), ON-TARGET plus Human FBXW7 pool (siFBXW7), ON-TARGET plus Human RHOA siRNA pool (siRhoA), ON-TARGET plus Human RHOB siRNA pool (siRhoB) and ON-TARGET plus Human FBXW7 siRNA – Set of 4 Upgrade (All GE-Healthcare/Dharmacon).

Cell culture

Primary human umbilical vein endothelial cells were isolated from umbilical cords which were obtained from the department of Obstetrics of the Amstelland ziekenhuis (Amstelveen, The Netherlands). Endothelial cells were isolated and cultured as described previously(40). Informed consents were obtained from all donors in accordance with the institutional guidelines and the Declaration of Helsinki. After Isolation cells of three different donors were pooled and cultured on 1% gelatin-coated plated in M199 medium supplemented with 100 U/ml penicillin and 100 µg/ml streptomycin, 2 mmol/L L-glutamine, 10% Heat-inactivated newborn calf serum (All Lonza, Verviers, Belgium) 10% heat-inactivated human serum (Invitrogen, WI), 150 µg/mL crude endothelial growth factor (prepared from bovine brains) and 5 U/mL heparin (Leo pharmaceutical products, Breda, The Netherlands). Cells were cultured at 37°C and 5% CO_2 with medium change every other day. For all experiments pools of 3 donors were used in passage 2 or 3.

HEK293T cells (ATCC) were cultured in Dulbecco's Modified Eagle Medium (Gibco) supplemented with penicillin 100 U/mL and streptomycin 100 µg/mL, L-glutamine 2 mM (All Lonza), 1 mM sodium pyruvate (Gibco) and 10% Fetal Bovine Serum (PAA).

esiRNA screen

A custom MISSION® esiRNA library (Sigma-Aldrich) targeting 62 human F-box proteins was ordered on a 96-well microtiter plate (Table 1). EGFP and KIF11 esiRNAs were used as controls. Sub-confluent p1 HUVECs were seeded on 1%-gelatin coated 96 W10idf ECIS arrays (Applied Biophysics, Troy, NY) in complete medium, 24 hours prior to transfection. Forward transfection of esiRNAs with dharmafect1 were performed according to the manufacturer's instructions using

esiRNA 100 ng final concentration and 0.2 % (v/v) of Dharmafect 1 transfection reagent (Dharmacon/GE-healtcare, Lafayette, CO) in 100 uL total volume. After 16 hours medium was replaced by normal culturing medium to avoid toxicity.

Transfection with small interfering RNA

HUVECs were transfected with Dharmafect1, according to the manufacturer's protocol (Dharmacon/GE-healthcare). Transfection was performed with a final concentration of 25 nM siRNA and 0.2% (v/v) Dharmafect 1 in 10% NBCSi/M199 per condition. Transfection was done on cells which were approximately 80% confluent in 96 wells, 12 wells and 6 wells format. Medium was replaced after 16 hours of transfection with regular cell culture medium to avoid toxicity.

Endothelial barrier function assays

Endothelial barrier function was measured with electrical cell-substrate impedance sensing (ECIS) and passage of Horse Radish Peroxidase (HRP).
For ECIS measurements, cells were seeded 1:1 density on gelatin coated 96 wells ECIS plates or 8 well arrays containing gold intercalated electrodes (Applied Biophysics). 24 Hours after seeding, cells were transfected using Dharmafect 1 and siRNAs for 16 hours. 72 hours after transfection, cells were serum-starved with M199 supplemented with 1% Human Serum Albumin (HSA, Sanquin CLP) for 90 minutes. Subsequently, a thrombin mix was added to the wells with a final concentration of 1U/mL (Sigma Aldrich). During the growth phase, resistance was measured at multiple frequencies to allow calculation for changes in cell-cell adhesion (Rb) and cell-matrix interaction (α).

For measurement of HRP passage, endothelial cells were transfected in a 6 or 12 wells plate for 24 hours before passaging 2:1 to 1% gelatin-coated 0.33 cm^2

polyester ThinCerts® cell culture inserts (Greiner Bio-one) with a pore-size of 3.0 µm. Approximately 72 hours after the start of transfection, cells were serum-starved with 1% HSA/M199 which was added to the filters for 60 minutes. Before stimulation, medium in the upper compartment was replaced with 1% HSA/M199 containing HRP 5 µg/mL (Sigma Aldrich) and 1U/mL thrombin or a vehicle control. 1% HSA/M199 was added to the lower compartment. A sample was taken from the lower compartment at different time points. The HRP concentration was calculated by measuring absorption after adding TetraMethylBenzidine (Upstate/Millipore) and sulfuric acid.

TritonX-114 protein extraction

This experiment was performed with some modifications according to Mohamed et al. (32). In brief, confluent monolayers of primary HUVECs seeded on 10 cm^2 culture wells were lysed on ice in Triton X-114 -containing lysis buffer [20 mM Tris-HCl(pH 7.5), 150 mM NaCl, 1% Triton X-114 and protease inhibitor cocktail (Roche). Cells were scraped and lysates were briefly centrifuged at 13,000 g. Triton X-114 insoluble pellet (P) was dissolved in sample buffer. Supernatant was carefully loaded on 6 % cushion solution (20 mM Tris-HCl (pH 7.4) 150 mM NaCl, 6% sucrose, 0.06% Triton X-114 and protease inhibitor cocktail) and incubated for 10 min at 37 C. After 5 min centrifugation at 16,000 g fractions were separated into aqueous (A) supernatant and detergent rich lipid containing droplet (D). All fractions were boiled with sample buffer and analyzed by immunoblotting. Previous to lysis HUVECs were transfected with control or FBXW7 siRNA pools as described before or treated with GGTI or FTI for 24 hours.

RhoB *in vivo* ubiquitination assay

HEK293T cells were co-transfected with mCherry-RhoB (18), HA-Ubiquitin (18) and FBXW7 plasmids (generous gift of C. Nicot, University of Kansas Medical Center, US) using Trans-IT-LT1 (Mirus) (#MIR 2300) following the manufacturer's protocol. Next day, cells were treated with 2.5 μM MG132 for the last four hours and denaturing HA-immunoprecipitation was performed as described previously (18).

Lentiviral shRNA FBXW7 knockdown and overexpression

For rescue experiment we transduced endothelial cells with shRNA targeting 3'UTR of FBXW7 (TRCN0000355644, Sigma Mission Library, Sigma Aldrich). Lentiviral particles were produced as by transfecting HEK293T cells with the third generation HIV-1 packaging plasmids (Addgene) using Trans-IT-LT1 (Mirus) as previously described (18). For FBXW7 lentiviral overexpression, doxocycline inducible pTripZ-FBXW7 (Generous gift of C. Nicot, University of Kansas Medical Center, US) was packed into lentiviral particles using the same protocol. To induce the expression of FBXW7 doxocycline (2 μg/ml) was added for 24 hours to the cell medium.

Immunoprecipitation of RhoB

Immunoprecipitation of endogenous RhoB was performed with rabbit αRhoB antibody (Santa Cruz) from confluent 60 cm2 dishes of primary HUVECs transfected with control siRNA or FBXW7 siRNA. Proteasomal degradation was inhibited by adding 5 μM MG132 at 2 hours before lysis. Upon stimulation, cells were washed in PBS containing 1 mM CaCl2 and 0.5 mM MgCl2 and lysed in lysis buffer (50mM Tris pH 7.4, 150mM NaCl, 1mM EDTA, 1 % NP40, Complete Protease Inhibitor Cocktail Tablets (Roche) and phosphatase inhibitors (1mM Na3VO4 and 25 mM NaF).

Lysates were cleared by centrifugation and incubated with 1 µg RhoB antibody for 2 hours at 4°C. RhoB containing complexes were pulled out by incubation with Dynabeads protein G (Thermo scientific) for 1 hour at 4°C. Finally, beads were washed 4 times with lysis buffer and immunoprecipitated proteins were eluted with sample buffer and analyzed with SDS-PAGE.

Protein analysis

To analyze protein levels, cells were seeded in 5 or 10 cm^2 culture wells and transfected as described above. 72 hours post transfection, cells were washed with cold PBS and whole-cell lysates were collected by scrapping the cells in the presence of 2x SDS sample buffer. Protein samples were loaded on 12,5% SDS-Page gels or NuPAGE Novex 4-12% Bis-Tris gels (Invitrogen), electrophoresed and transferred to nitrocellulose membranes. Protein analysis was performed by incubation of the nitrocellulose membranes with the designated antibodies. Bands were visualized with enhanced chemiluminescence (Amersham/GE-healthcare) on an AI600 machine (Amersham/GE-healthcare).

Immunofluorescent imaging of cultured endothelial cells

Transfected cells were seeded on 2 cm^2 and 12 mm glass coverslips (Menzel), coated with 1% gelatin and crosslinked with 0.5% glutaraldehyde (Sigma Aldrich), approximately 24 hours after the start of transfection. Cells were grown for 48 hours with complete medium to reach the transfection time of 72 hours. After pre-incubating with 1% HSA/M199 for 1 hour, thrombin was added to the wells in a final concentration of 1U/mL. After 15 minutes or 3 hours, cells were fixed with warm (37 °C) 4% paraformaldehyde (Sigma Aldrich) and put on ice for 15 minutes. The PFA was washed away with phosphate buffered saline (PBS) and cells were

permeabilized with 0.2% Triton X-100 in PBS (Sigma Aldrich) and blocked for 30 minutes with 1% BSA. Hereafter, coverslips were stained with primary antibodies against VE-cadherin or RhoB (in 0.1% BSA/PBS) for 1 hour at room temperature. After washing 3 times, the cells were incubated with a FITC-labeled secondary antibody (anti-rabbit or anti-mouse 1:100 in 0.1% BSA/PBS) and acti stain phalloidin (direct staining, in 0.1% BSA/PBS (Tebu Bio)) at room temperature. After washing, the cells were incubated with DAPI (Thermo Fisher Scientific) at room temperature. Coverslips were mounted with Mowiol4-88/DABCO solution (Calbiochem, Sigma Aldrich). Confocal scanning laser microscopy was performed on a Nikon A2R confocal microscope (Nikon). Images were analyzed and equally adjusted with ImageJ.

RNA Isolation and Quantitative Polymerase Chain Reaction

Isolation of total RNA and subsequent real-time quantitative polymerase chain reaction was done as previously reported(41). Sequences of quantitative polymerase chain reaction primers are available on request.

Statistical analysis

For the esiRNA screen the observed values (n=4) were compared with the EGFP controls by a student t-test. Hereafter, the p-values were corrected for multiple testing by using a Benjamini-Hochberg false-discovery rate (FDR) set to <0.05.

For the other experiments, data is represented as mean±SEM unless indicated otherwise. Comparison of 2 conditions was tested by student's t-test. Comparison of more than 2 conditions was tested by 1-way ANOVA or repeated measures ANOVA with Dunnet's posthoc test. P-values were considered statistically significant if $P<0.05$. Analysis was performed using Graphpad Prism software.

References

1. Lee WL, Slutsky AS. Sepsis and endothelial permeability. N Engl J Med. 2010;363(7).
2. Dejana E. Endothelial adherens junctions Implication in the control of vascular permeability and angiogenesis. J Clin Invest. 1996;98(9):1949-53.
3. Giannotta M, Trani M, Dejana E. VE-cadherin and endothelial adherens junctions: active guardians of vascular integrity. Dev Cell. 2013;26(5):441-54.
4. Abu Taha A, Schnittler H-J. Dynamics between actin and the VE-cadherin/catenin complex. Cell Adhesion & Migration. 2014;8(2):125-35.
5. Hordijk PL, Anthony E Fau - Mul FP, Mul Fp Fau - Rientsma R, Rientsma R Fau - Oomen LC, Oomen Lc Fau - Roos D, Roos D. Vascular-endothelial-cadherin modulates endothelial monolayer permeability. 1999(0021-9533 (Print)).
6. Wojciak-Stothard B, Ridley AJ. Rho GTPases and the regulation of endothelial permeability. Vascular Pharmacology. 2002;39(4-5):187-99.
7. Van Nieuw Amerongen GP, Van Delft S, Vermeer MA, Collard JG, Van Hinsbergh VW. Activation of RhoA by Thrombin in Endothelial Hyperpermeability -Role of Rho Kinase and Protein Tyrosine Kinases. Circ Res. 2000;87:335-40.
8. Cherfils J, Zeghouf M. Regulation of small GTPases by GEFs, GAPs, and GDIs. Physiol Rev. 2013;93(1):269-309.
9. Bos JL, Rehmann H, Wittinghofer A. GEFs and GAPs: Critical Elements in the Control of Small G Proteins. Cell. 2007;129(5):865-77.
10. Garcia-Mata R, Boulter E, Burridge K. The 'invisible hand': regulation of RHO GTPases by RHOGDIs. Nat Rev Mol Cell Biol. 2011;12(8):493-504.
11. Schaefer A, Reinhard NR, Hordijk PL. Toward understanding Rho GTPase specificity: structure, function and local activation. Small GTPases. 2014;5(2):6.
12. Hodge RG, Ridley AJ. Regulating Rho GTPases and their regulators. Nat Rev Mol Cell Biol. 2016.
13. Adamson P, Marshall CJ, Hall A, Tilbrook PA. Post-translational modifications of p21Rho proteins. Biol Chem. 1992;267(28):20033-8.
14. Von Zee CL, Stubbs EB, Jr. Geranylgeranylation facilitates proteasomal degradation of rho G-proteins in human trabecular meshwork cells. Invest Ophthalmol Vis Sci. 2011;52(3):1676-83.
15. Mazieres J, Tillement V, Allal C, Clanet C, Bobin L, Chen Z, et al. Geranylgeranylated, but not farnesylated, RhoB suppresses Ras transformation of NIH-3T3 cells. Exp Cell Res. 2005;304(2):354-64.
16. Duluc L, Ahmetaj-Shala B, Mitchell J, Abdul-Salam VB, Mahomed AS, Aldabbous L, et al. Tipifarnib prevents development of hypoxia-induced pulmonary hypertension. Cardiovasc Res. 2017;113(3):276-87.
17. Wei J, Mialki RK, Dong S, Khoo A, Mallampalli RK, Zhao Y, et al. A new mechanism of RhoA ubiquitination and degradation: roles of SCF(FBXL19) E3 ligase and Erk2. Biochim Biophys Acta. 2013;1833(12):2757-64.
18. Kovačević I, Sakaue T, Majoleé J, Pronk MC, Maekawa M, Geerts D, et al. The Cullin-3–Rbx1–KCTD10 complex controls endothelial barrier function via K63 ubiquitination of RhoB. Journal of cell Biology. 2018;217(2):1015-32.
19. Pickart CM, Eddins MJ. Ubiquitin: structures, functions, mechanisms. Biochim Biophys Acta. 2004;1695(1-3):55-72.
20. Ardley HC, Robinson PA. E3 ubiquitin ligases. Biochemistry. 2005;41:15-30.
21. Cardozo T, Pagano M. The SCF ubiquitin ligase: insights into a molecular machine. Nat Rev Mol Cell Biol. 2004;5(9):739-51.
22. Zhou ZD, Sathiyamoorthy S, Angeles DC, Tan EK. Linking F-box protein 7 and parkin to neuronal degeneration in Parkinson's disease (PD). Mol Brain. 2016;9:41.
23. Wang Z, Liu P, Inuzuka H, Wei W. Roles of F-box proteins in cancer. Nat Rev Cancer. 2014;14(4):233-47.
24. Izumi N, Helker C, Ehling M, Behrens A, Herzog W, Adams RH. Fbxw7 controls angiogenesis by regulating endothelial Notch activity. PLoS One. 2012;7(7):e41116.

25. Wang R, Wang Y, Liu N, Ren C, Jiang C, Zhang K, et al. FBW7 regulates endothelial functions by targeting KLF2 for ubiquitination and degradation. Cell Res. 2013;23(6):803-19.
26. Moy AB, Winter M, Kamath A, Blackwell K, Reyes G, Giaever I, et al. Histamine alters endothelial barrier function at cell-cell and cell-matrix sites. Am J Physiol Lung Cell Mol Physiol. 2000;278(5).
27. Pronk MCA, van Bezu JSM, van Nieuw Amerongen GP, van Hinsbergh VWM, Hordijk PL. RhoA, RhoB and RhoC differentially regulate endothelial barrier function. Small GTPases. 2017:1-19.
28. Li H, Wang Z, Zhang W, Qian K, Xu W, Zhang S. Fbxw7 regulates tumor apoptosis, growth arrest and the epithelial-to-mesenchymal transition in part through the RhoA signaling pathway in gastric cancer. Cancer Lett. 2016;370(1):39-55.
29. Loregger A, Raaben M, Tan J, Scheij S, Moeton M, van den Berg M, et al. Haploid Mammalian Genetic Screen Identifies UBXD8 as a Key Determinant of HMGCR Degradation and Cholesterol Biosynthesis. Arterioscler Thromb Vasc Biol. 2017;37(11):2064-74.
30. Sundqvist A, Bengoechea-Alonso MT, Ye X, Lukiyanchuk V, Jin J, Harper JW, et al. Control of lipid metabolism by phosphorylation-dependent degradation of the SREBP family of transcription factors by SCF(Fbw7). Cell Metab. 2005;1(6):379-91.
31. Stamatakis K, Cernuda-Morollon E, Hernandez-Perera O, Perez-Sala D. Isoprenylation of RhoB is necessary for its degradation. A novel determinant in the complex regulation of RhoB expression by the mevalonate pathway. J Biol Chem. 2002;277(51):49389-96.
32. Mohamed A, Viveiros A, Williams K, Posse de Chaves E. Abeta inhibits SREBP-2 activation through Akt inhibition. J Lipid Res. 2018;59(1):1-13.
33. Kainulainen M, Lau S, Samuel CE, Hornung V, Weber F. NSs Virulence Factor of Rift Valley Fever Virus Engages the F-Box Proteins FBXW11 and beta-TRCP1 To Degrade the Antiviral Protein Kinase PKR. J Virol. 2016;90(13):6140-7.
34. Machida Yj Fau - Machida YJ, Dutta A Fau - Dutta A. The APC/C inhibitor, Emi1, is essential for prevention of rereplication. Genes & Development. 2007;21(2):184-94.
35. Penter L, Maier B, Frede U, Hackner B, Carell T, Hagemeier C, et al. A rapid screening system evaluated novel inhibitors of DNA methylation and suggest F-box proteins as potential therapeutic targets for high-risk neuroblastoma. Targeted Oncology. 2015;10(4):523-33.
36. Tsunematsu R, Nakayama K, Oike Y, Nishiyama M, Ishida N, Hatakeyama S, et al. Mouse Fbw7/Sel-10/Cdc4 is required for notch degradation during vascular development. J Biol Chem. 2004;279(10):9417-23.
37. Onoyama I, Suzuki A, Matsumoto A, Tomita K, Katagiri H, Oike Y, et al. Fbxw7 regulates lipid metabolism and cell fate decisions in the mouse liver. J Clin Invest. 2011;121(1):342-54.
38. Wherlock M, Gampel A, Futter CE, Mellor H. Farnesyltransferase inhibitors disrupt EGF receptor traffic through modulation of the RhoB GTPase. Journal of Cell science. 2004;117:3221-31.
39. Du W, Lebowitz PF, Prendergast GC. Cell growth inhibition by Farnesyltransferase inhibitors is mediated by gain of geranylgeranylated RhoB. Mol Cell Biol. 1999;19(3):1831-40.
40. Jaffe EA, Nachman RL, Becker CG, Minick CR. Culture of Human Endothelial cells derived from Umbilical veins. j Clin Invest. 1973;52(11):2745-56.
41. Loregger A, Cook EC, Nelson JK, Moeton M, Sharpe LJ, Engberg S, et al. A MARCH6 and IDOL E3 Ubiquitin Ligase Circuit Uncouples Cholesterol Synthesis from Lipoprotein Uptake in Hepatocytes. Mol Cell Biol. 2015;36(2):285-94.
42. Bolte S, Cordelieres FP. A guided tour into subcellular colocalization analysis in light microscopy. J Microsc. 2006;224(Pt 3):213-32.

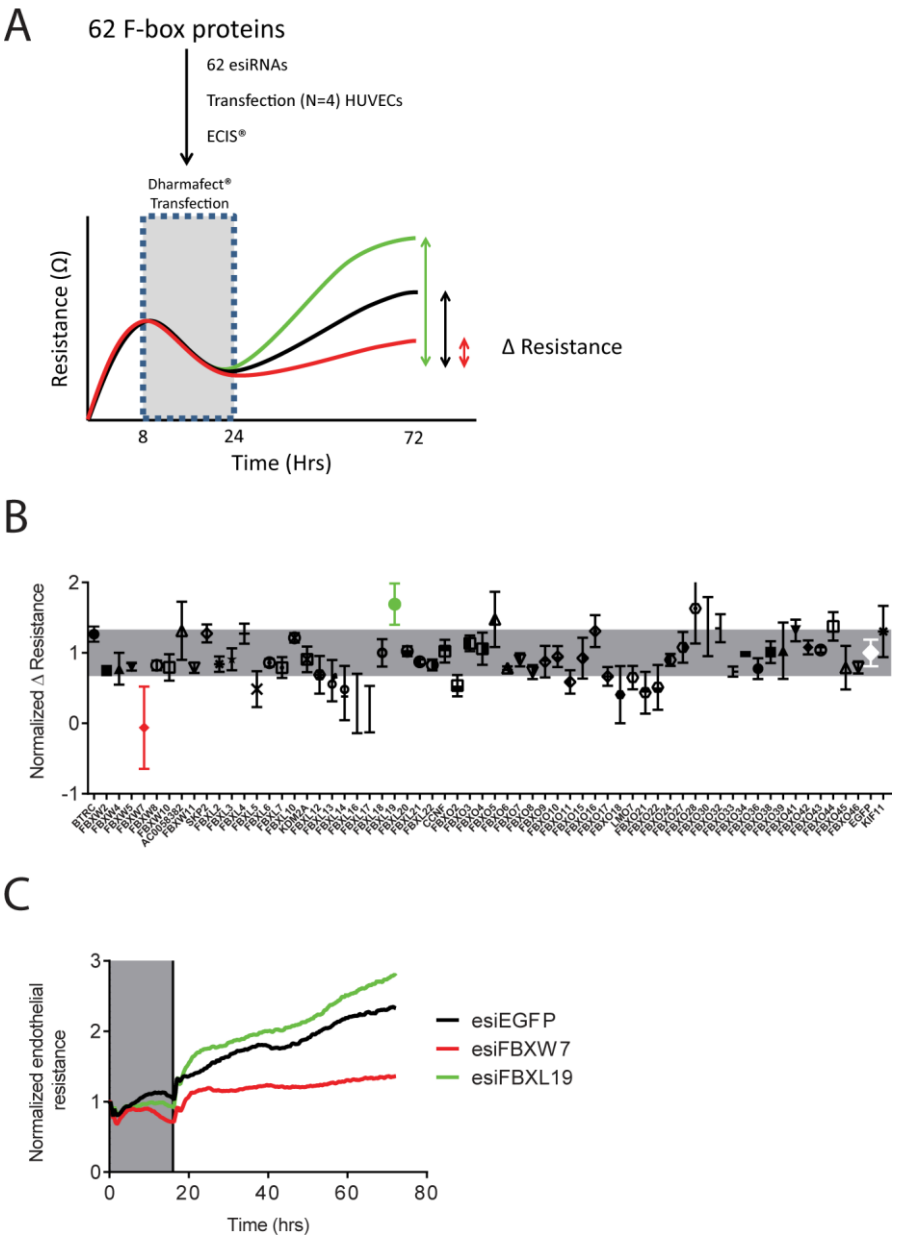

Figure 1 – esiRNA screen identifies Fbox proteins involved in endothelial barrier function

A) Schematic representation of the esiRNA screen. 62 esiRNAs were transfected into pools of HUVECs seeded on 96W10idf ECIS arrays (n=4). Endothelial resistance was measured for 72 hours following transfection. A schematic ECIS graph is shown. In green, an example for the enhancement of the endothelial barrier after knockdown is shown. In red an example of disruption of the endothelial barrier after knockdown is

shown and in black a control EGFP esiRNA is presented. B) Overview of the mean delta of electrical resistance from the start of transfection until the 72 hour time point for each esiRNA. The EGFP control is depicted in white, in green the highest value is depicted, in red the lowest value is depicted. The grey bar represents the threshold value at ± 33% of the EGFP control. Datapoints represent mean±SEM (N=4). C) Effect of loss of FBXL19, EGFP and FBXW7 on basal endothelial barrier function. Data represent normalized average values from the start of transfection (T=0) until the end of the experiment of n=4 experiments.

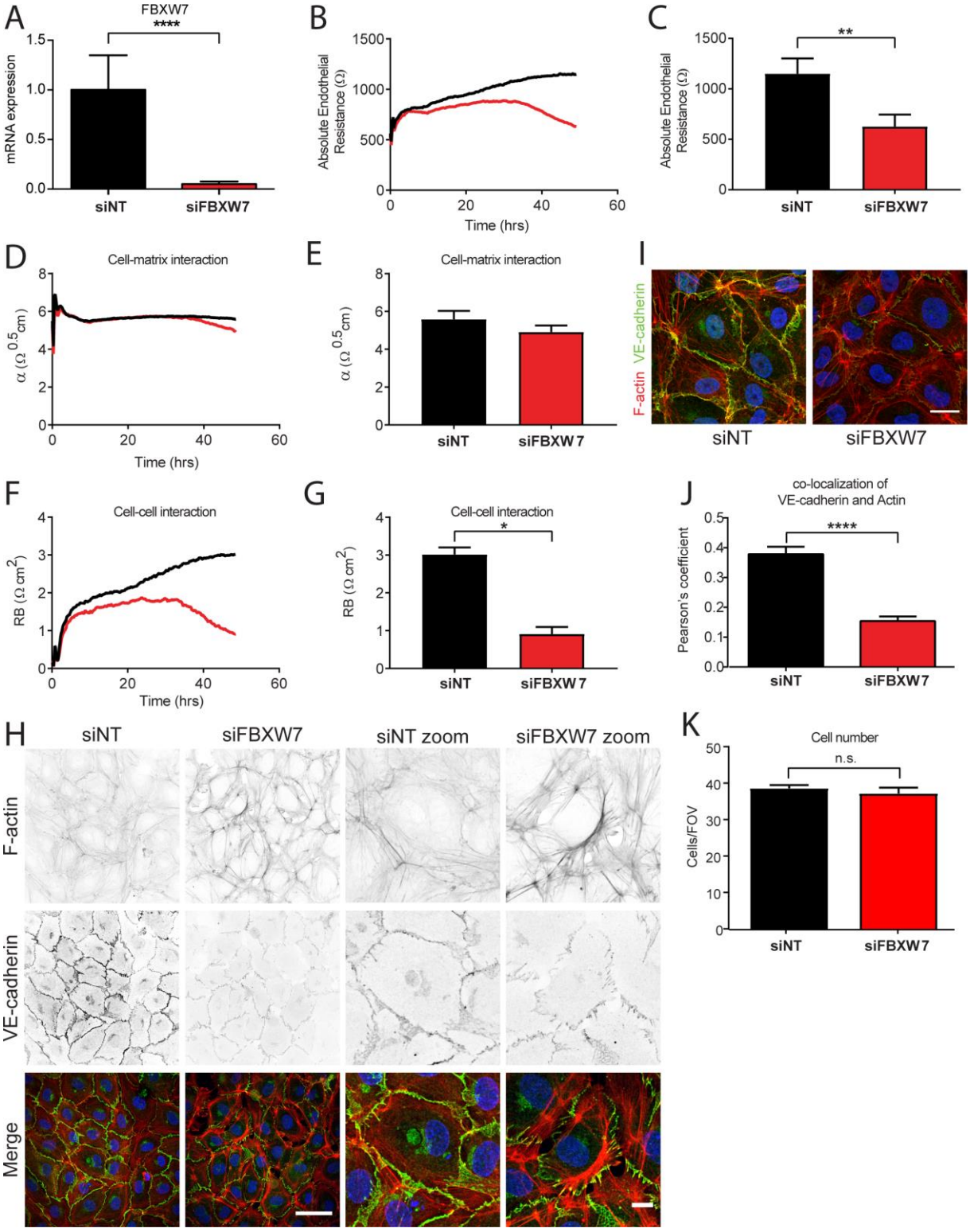

Figure 2 – FBXW7 knockdown causes decreased endothelial barrier function by increased contractile ring formation

A) HUVECs were transfected with siNT and siFBXW7 and cultured for 72 hours. Total RNA was isolated, and expression of the indicated genes was determined by quantitative polymerase chain reaction. Each bar and error represent the mean±SD (n=3); **** p<0.0001 B) Effect of the loss of FBXW7 on basal endothelial barrier function. C) Basal endothelial barrier function at t=72 hours. D) Absolute endothelial resistance attributable to cell-matrix adhesion (α) of control and FBXW7 knockdown cells. E) α at t=72 hours. F) Absolute endothelial resistance attributable to cell-cell adhesion (Rb) of control and FBXW7 knockdown cells. G) Rb at t=72 hours. H) Immunofluorescent staining of VE-cadherin (green), F-actin (red) and nuclei (blue) in HUVECs for visualization of adherens junctions and actin fibers following loss of FBXW7. Scale bar, 50 μM. In the zoomed images, scale bar, 10 μM. Representative images of 3 experiments. I) Immunofluorescent staining of VE-cadherin (green), F-actin (red) and nuclei (blue) in HUVECs for visualization of co-localization of adherens junctions and actin fibers following loss of FBXW7.. Scale bar, 20 μM. J) Quantification of Mander's coefficient of colocalization of VE-cadherin with actin from I) was performed using ImageJ and JACoP plugin (42) (N=12). K) Cell number quantification in control and FBXW7 knockdown cells at t=72 hours. DAPI stained nuclei were counted per field of view (N=12). ECIS data represent average values (line graphs, representing barrier formation, Rb or α from medium change at 16 hours after transfection (t=0) until the end of the experiment) or mean±SEM (bar graphs) of N=3 experiments. * p<0,05 ** p<0.01 paired t-test. Co-localization data represent mean±SEM of N=3 experiments. **** p<0,0001 unpaired t-test. siNT, non-targeting siRNA.

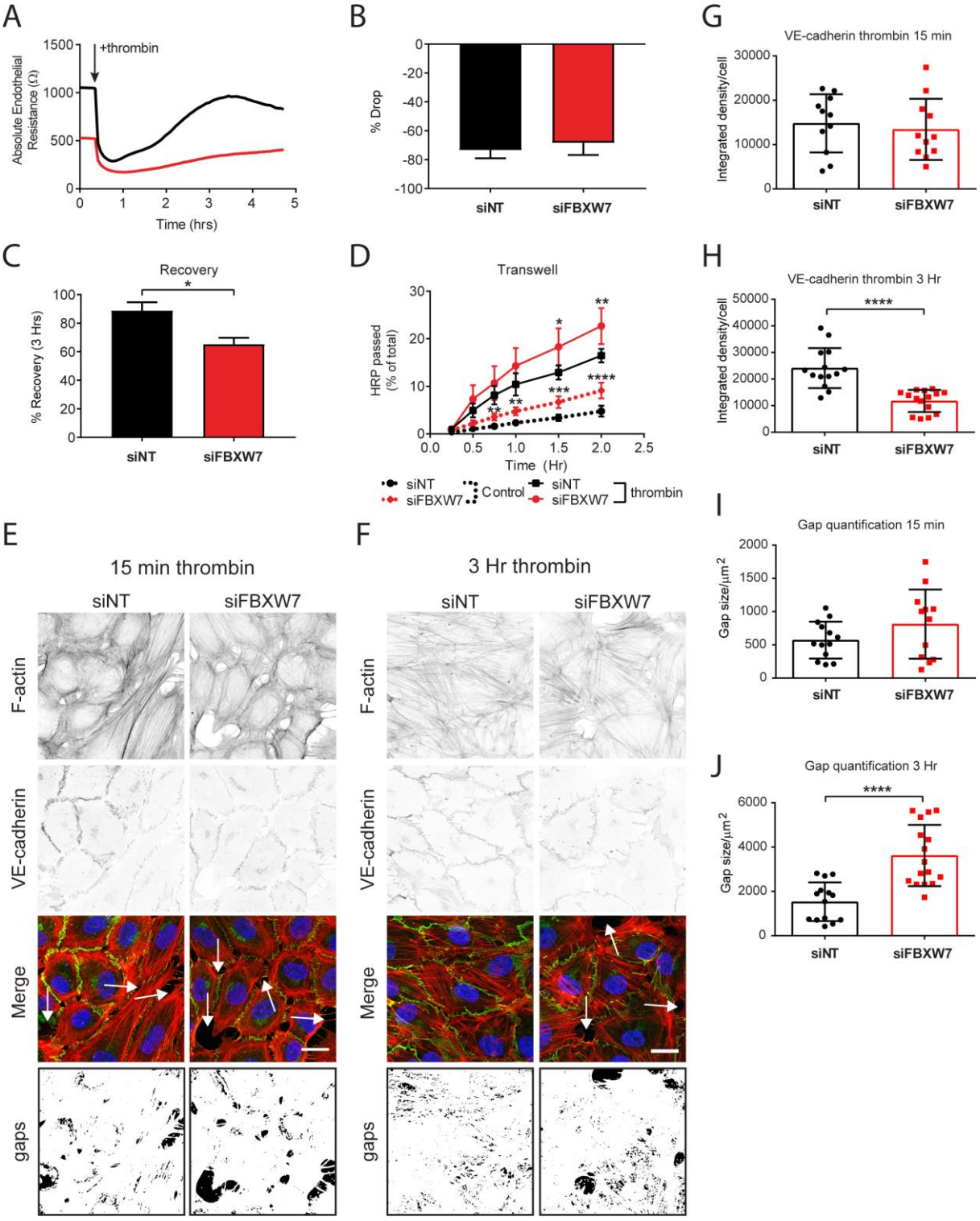

Figure 3 – The effect of thrombin-induced hyper-permeability on FBXW7 knockdown cells

A) Thrombin-induced endothelial barrier disruption in FBXW7 knockdown cells. Arrow indicates addition of Thrombin (1U/mL). B) The thrombin response (% decrease in

normalized resistance) in control versus FBXW7 knockdown cells. Values represents the percentage drop at the lowest point of resistance following the addition of thrombin. C) The % recovery at 3 hours after thrombin relative to the respective start values in control versus FBXW7 knockdown cells. D) Time-dependent effects of control and FBXW7 knockdown on the passage of HRP across control and thrombin-stimulated HUVECs. Data represent average of 3 experiments. E,F) Immunofluorescent staining of VE-cadherin (green), F-actin (red) and nuclei (blue) in HUVECs for visualization of adherens junctions and actin fibers following loss of FBXW7 and after 15 minutes (E) and 3 hours (F) of thrombin stimulation. Arrows indicate gaps. Scale bars, 20 μM. Images are representative of 3 experiments. G,H) Quantification of VE-cadherin staining intensity at 15 min (G) and 3 hours (H) after thrombin stimulation. Integrated density of VE-cadherin staining per cell was calculated using ImageJ software. N=12. I,J) Quantification of inter-endothelial gap size at 15 min (I) and 3 hours (J) after thrombin stimulation. Gap size was measured using ImageJ software. ECIS data represent average values or mean±SEM (bar graphs) of N=3 experiments. * $p<0,05$ paired t-test. Panel D shows average values of 3 experiments performed in triplicates. *$p<0.05$, ** $p<0.01$, *** $p<0.001$, **** $p<0.0001$ in Dunnett's post-hoc analysis of 2 way ANOVA multiple comparisons test. siNT, non-targeting siRNA

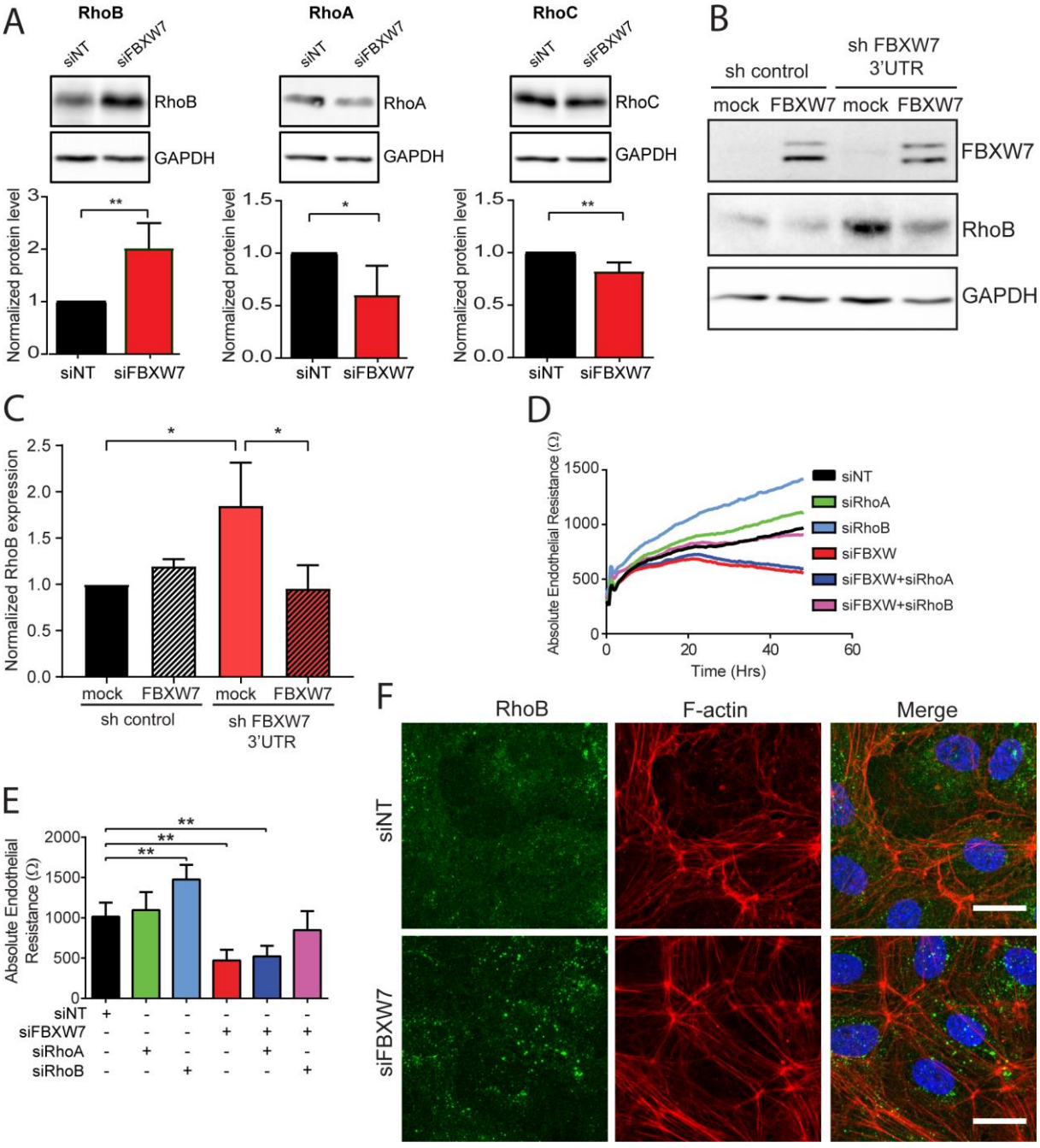

Figure 4 – FBXW7 knockdown increased RhoB levels in HUVECs

A) Western blot of whole cell lysates showing the effect of FBXW7 knockdown on expression of RhoB, RhoA and RhoC in HUVECs. Representative blots from 4 experiments is shown. GAPDH is included as a loading control. Bar graph represents mean±SD of RhoB expression from 4 individual experiments, all relative to GAPDH and normalized to siNT. B) Western blot of the FBXW7 rescue experiment. Cells

were infected with control lentivirus or lentivirus carrying shRNA which targets 3'UTR of FBXW7 mRNA in combination with lentivirus carrying empty pTRIPZ doxocycline inducible vector or pTRIPZ vector containing FBXW7 cDNA. Doxocycline was added 24 hours before cell lysis. GAPDH is shown as loading control. C) Quantification of the RhoB levels from B). Bar graphs represent mean±SD of RhoB expression from 3 individual experiments, all relative to GAPDH and normalized to sh control + mock condition. D,E) Effect of loss of RhoA, RhoB in combination with FBXW7 knockdown on basal endothelial barrier function. E) Quantification of basal endothelial barrier function at t=72 hours. F) Immunofluorescent staining of RhoB (green), F-actin (red) and nuclei (blue) in control and FBXW7 knockdown HUVECs. Scale bar, 20 μM. Images are representative of 3 experiments. ECIS data represent average values (line graphs, representing barrier formation from medium change at 16 hours after transfection (t=0) until the end of the experiment) or mean±SEM (bar graphs) of N=4 experiments. * $p<0,05$ Paired t-test. ** $p<0.01$ in Dunnett's post-hoc analysis of one-way ANOVA.

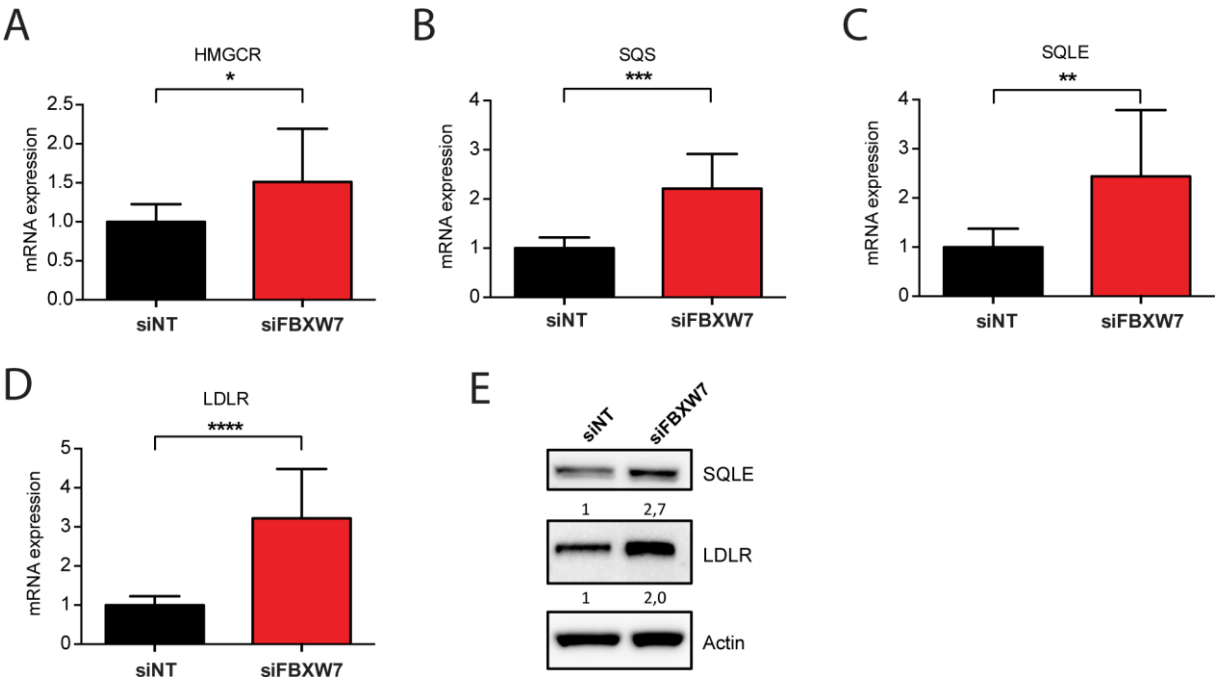

Figure 5 – FBXW7 knockdown induces activation of the cholesterol synthesis pathway

(A-D) HUVECs were transfected with siNT and siFBXW7 and cultured for 72 hours. Total RNA was isolated, and expression of the indicated genes was determined by quantitative polymerase chain reaction. Each bar and error represent the mean±SD (n=3); * $p<0.05$, ** $p<0.01$, *** $p<0.001$, **** $p<0.0001$ E) Western blot of whole cell lysates showing the effect of FBXW7 knockdown on expression of SQLE and LDLR in HUVECs. Representative blots from 4 experiments are shown. Actin is included as a loading control. Numbers represent mean from 4 individual experiments all normalized to siNT.

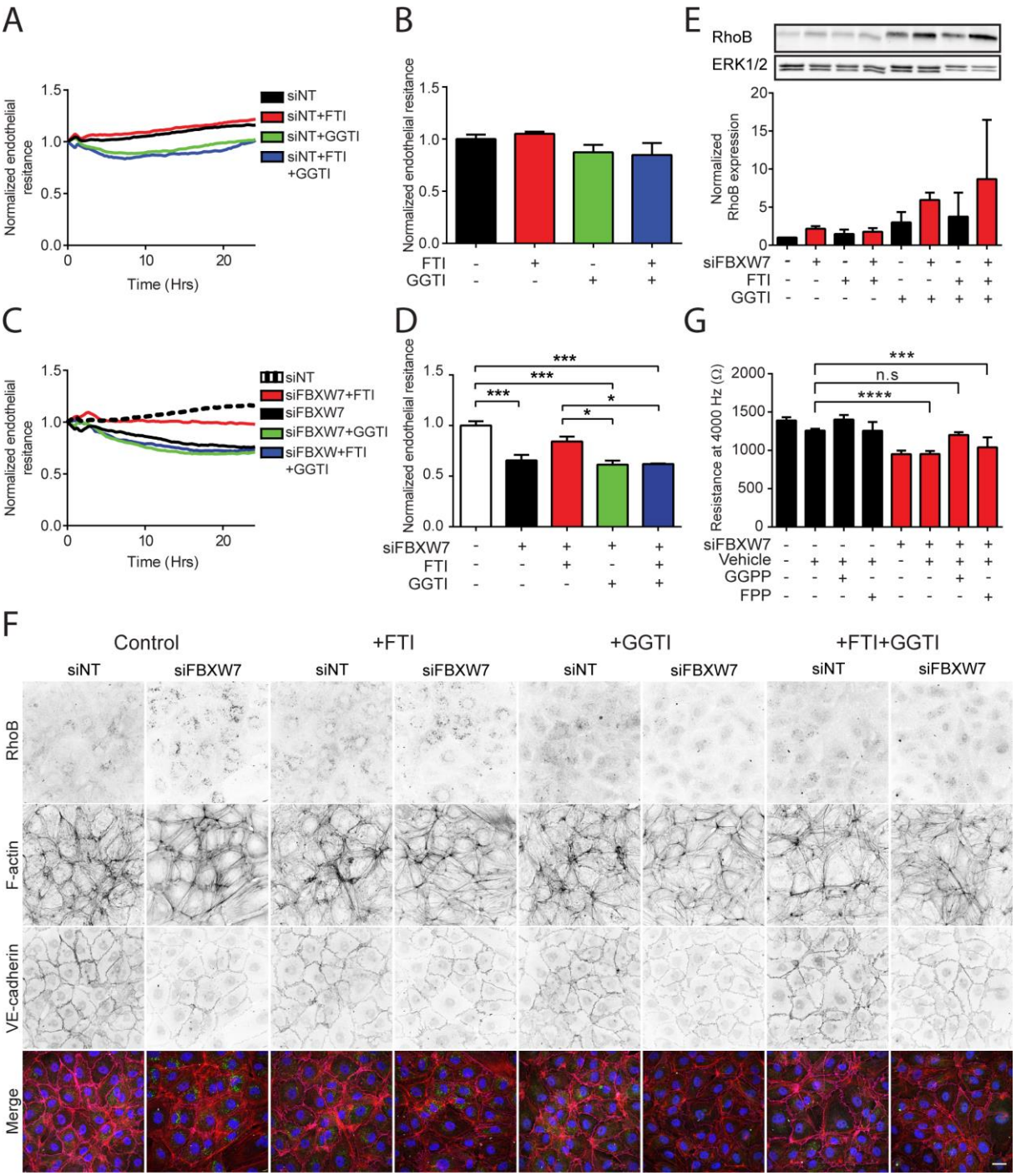

Figure 6 – Endothelial barrier disruption is caused by impaired prenylation of RhoB in FBXW7 knockdown cells

A) Effect of farnesyl transferase inhibitor (FTI;10 μM; red), Geranylgeranyl transferase inhibitor (GGTI;10 μM; green) and the combination (blue) on normalized barrier function of control cells. T=0 corresponds to 48 hours after transfection. B)

Endothelial barrier function after 24 hours stimulation with FTI + GGTI. C) Effect of addition of farnesyl transferase inhibitor (FTI; red), Geranylgeranyl transferase inhibitor (GGTI; green) and combination (blue) on normalized barrier function of FBXW7(black) knockdown and control (dashed) cells. T=0 is 48 hours after transfection. D) Endothelial barrier function after 24 hours stimulation with FTI + GGTI). E) Western blot of whole cell lysates showing the effect of FBXW7 knockdown and stimulation with FTI and GGTI on expression of RhoB in HUVECs. Representative blots from 2 experiments are shown. ERK1/2 is included as a loading control. Bar graph represents mean±sd from 2 individual experiments all normalized to siNT. F) Immunofluorescent staining of RhoB (green), F-actin (red), VE-cadherin (magenta) and nuclei (blue) in control and FBXW7 knockdown HUVECs stimulated with FTI, GGTI or combination. Scale bar, 25 μM. Images are representative of 3 individual experiments. G) Effect of Geranylgeranyl pyrophosphate (GGPP;10 μM) and Farnesyl pyrophosphate (FPP;10 μM) on barrier function of control and FBXW7 knockdown cells. Data represents mean±SD of n=2 experiments performed in triplicate. A-D data represent average values (line graphs, representing barrier function from addition of inhibitor 48 hours after transfection (T=0) until the end of experiment) or mean±SEM of N=3 experiments performed in duplicates. * $p<0.05$, *** $p<0.001$, **** $p<0.0001$ in Dunnett's post-hoc analysis of one-way ANOVA.

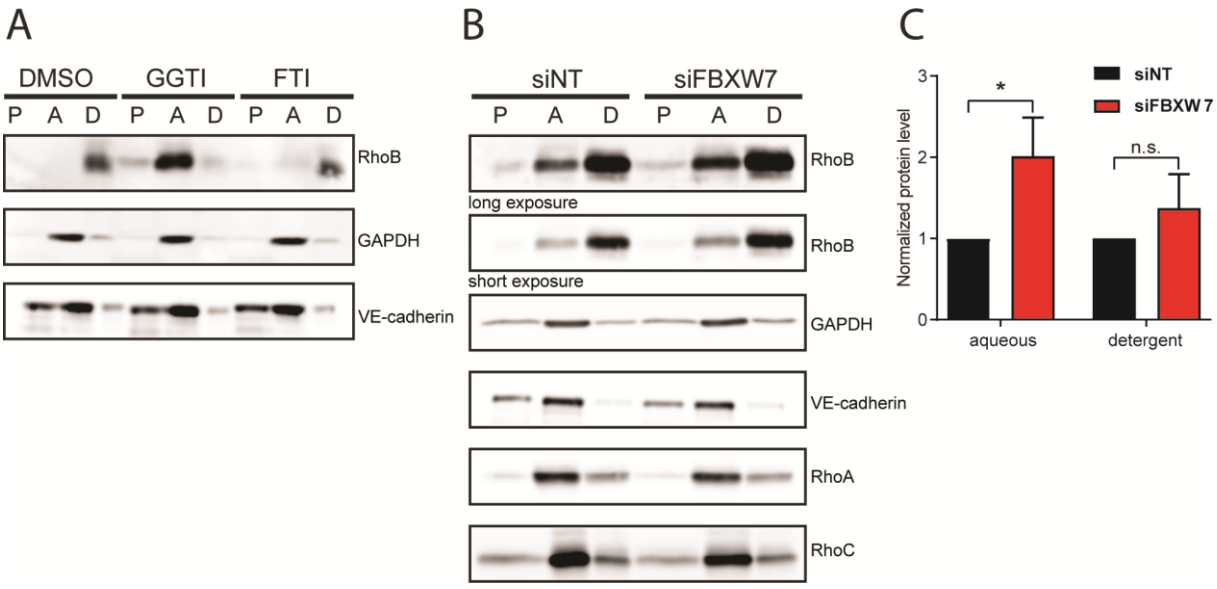

Figure 7 - FBXW7 knockdown mimics impairment in RhoB prenylation induced by GGTI treatment A) Western blot showing RhoB expression in protein fractions obtained from HUVECs after TritonX-114 extraction followed by centrifugation on 6 % sucrose cushion solution. The cells were pre-treated with DMSO, GGTI or FTI for 18 hours. P-triton insoluble pellet, A- aqueous fraction and D- detergent rich lipid droplet. GAPDH is shown as loading control. B) Western blot of RhoA, RhoB and RhoC in samples obtained as in A from HUVECs transfected with control or FBXW7 siRNA at 72 hours post transfection. C) Quantification of RhoB immunoblot from B. Bar graph represents mean±SD of RhoB expression in aqueous and detergent rich fraction from 3 individual experiments, all relative to GAPDH and normalized to siNT.

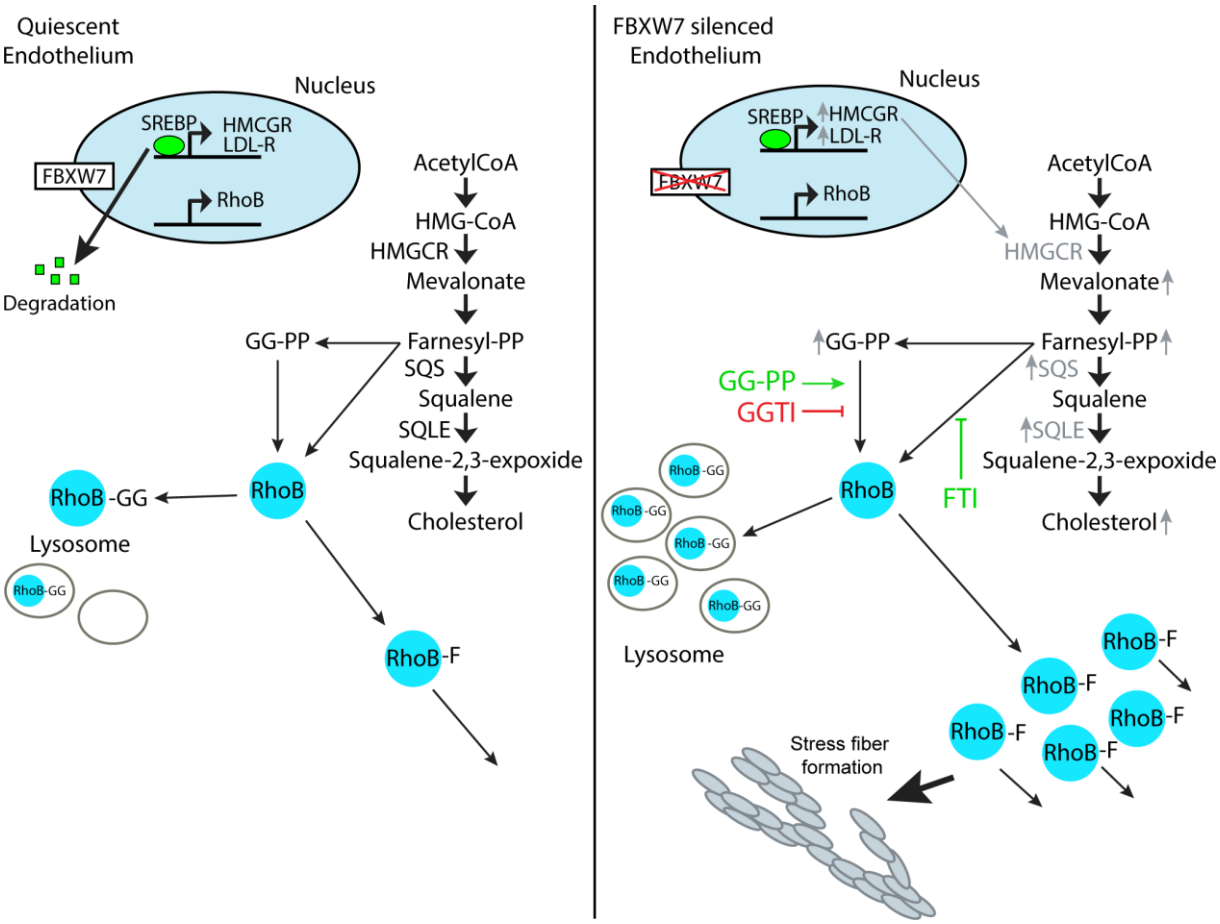

Figure 8 – Proposed model of regulation of endothelial barrier function by FBXW7

In quiescent endothelium, SREBP is efficiently degraded via the proteasome because of FBXW7-mediated ubiquitination, so there is no or little activation of the cholesterol pathway. RhoB is expressed at low levels, the expressed RhoB is modified with a geranylgeranyl group to be inactive and stored in vesicles, or with a farnesyl group to be active at the cell periphery. Upon loss of FBXW7, SREBP is stabilized, which results in activation of the cholesterol pathway by induction of HMCGR. Therefore, there is more geranylgeranyl pyrophosphate and farnesyl pyrophosphate generated to modify RhoB. More RhoB will accumulate in the vesicles but also more RhoB will be active at the cell periphery, inducing stress fiber formation and contraction. Addition of FTI will rescue this effect because this induces geranylgeranylation of RhoB, an effect which is mimicked by GGPP. Addition of GGTI will lead to a switch towards farnesylation of RhoB which promotes its signaling at the plasma membrane and thus is detrimental for endothelial barrier function.

Table 1 – List of F-box proteins included in the screen. esiRNA targeted F-box proteins are grouped into three protein families: F-box and Leucine-rich repeat (FBXL), F-box only (FBXO) and F-box and WD40 domain (FBXW). esiRNAs targeting 19 FBXL, 34 FBXO and 9 FBXW proteins were included in the screen.

FBXL	FBXO		FBXW
SKP2	CCNF	FBXO27	BTRC
FBXL2	FBXO2	FBXO28	FBXW2
FBXL3	FBXO3	FBXO30	FBXW4
FBXL4	FBXO4	FBXO32	FBXW5
FBXL5	FBXO5	FBXO33	FBXW7
FBXL6	FBXO6	FBXO34	FBXW8
FBXL7	FBXO7	FBXO36	FBXW10
FBXL10	FBXO8	FBXO38	AC005838.2
KDM2A	FBXO9	FBXO39	FBXW11
FBXL12	FBXO10	FBXO41	
FBXL13	FBXO11	FBXO42	
FBXL14	FBXO15	FBXO43	
FBXL16	FBXO16	FBXO44	
FBXL17	FBXO17	FBXO45	
FBXL18	FBXO18	FBXO46	
FBXL19	LMO7		
FBXL20	FBXO21		
FBXL21	FBXO22		
FBXL22	FBXO24		